

# Numerical Analysis of Laser Produced Plasma Expansion with Large Ion Larmor Radius via 3D PIC Simulation

Masanori NUNAMI<sup>1,3)</sup> and Katsunobu NISHIHARA<sup>2)</sup>

<sup>1)</sup>Research Institute for Sustainable Humanosphere, Kyoto University, Kyoto 611-0011, Japan

<sup>2)</sup>Institute of Laser Engineering, Osaka University, Osaka 565-0871, Japan

<sup>3)</sup>Japan Science and Technology Agency, CREST, Saitama 332-0012, Japan

(Received: 2 September 2008 / Accepted: 19 November 2008)

Expansion phenomena of laser produced cluster plasma in an external strong magnetic field have been studied. In the cluster plasma expansion process, the ion Larmor radius is often much larger than the initial cluster size, while the electron Larmor radius is smaller than the cluster size, namely,  $R_e < R_0 \ll R_i$ , where  $R_{e(i)}$  is Larmor radius of electron (ion) and  $R_0$  is the initial cluster size. We applied a 3D full Particle-In-Cell simulation code to the laser produced cluster plasma in an external strong magnetic field and discussed the simulation results. Because of the ion large Larmor radius, accelerated ions get ahead of the electron surface and generate inward-directed radial electric field. Therefore magnetized electron surface separates from the ion surface. The surface of magnetized electrons is unstable for the flute type instability mainly due to the inward-directed electric field created by streaming ions with large Larmor radii. However we found that the ion surface is relatively stable which is a new result compared with the previous works.

Keywords: Laser produced plasma, Large Larmor radius, Rayleigh-Taylor instability, PIC, LPP-EUV

## 1. Introduction

Understanding for expansion mechanism of laser produced plasma (LPP) into a magnetic field is very important in studies of inertial confinement fusion plasma, developments of LPP extreme ultra violet (LPP-EUV) light source [1] with ion debris mitigation by external magnetic field, and so on. Expanding plasma into a magnetic field would meet with several instabilities as the Rayleigh-Taylor instability, which is originally formulated for ordinary fluids with a heavy fluid supported by a less dense fluid [2]. The analogies of the Rayleigh-Taylor instability with MHD plasma were formulated in the 1950s. In contrast, when the ion Larmor radii become large compared with a density gradient length, i.e., the ions are unmagnetized although the electrons are magnetized, the Rayleigh-Taylor-like instability occurs with the different growth mechanism comparing with conventional MHD-Rayleigh-Taylor instability. In this paper, we focused the ion large Larmor radius (LLR) regime, simulated the expansion phenomena of LPP in a magnetic field by 3D full particle-in-cell (PIC) simulation and discussed the growth of the Rayleigh-Taylor-like instability and nonlinear phenomena of the LPP expansion.

## 2. Instability in LLR regime

In conventional MHD-Rayleigh-Taylor instability, ions and electrons drift in direct response to the effective gravitational force with opposite directions each other. The ion-electron mass ratio is large, the result-

ing charge separation generates local electric fields,  $\delta\mathbf{E}$ , and drives the growth of perturbation amplitude through  $\delta\mathbf{E} \times \mathbf{B}$  drift. On the other hand, in LLR regime, the growth mechanism is much different. In LPP expansion process with external magnetic field, since initial electron pressure of the laser heated cluster plasma is much higher than magnetic pressure, electrons first expand into the vacuum. And then electrons perform gyro motion with their small Larmor radii. Ions are accelerated outward due to electric field generated by the expanding electrons. Then ions can get ahead of the electron surface and generate inward-directed electric fields  $\mathbf{E}_r$  as in Fig.1. Due to the inward electric field, ions are decelerated in cross-field direction, and cross-field energy of the ion is suppressed. The electrons respond to  $\mathbf{E}_r \times \mathbf{B}$  drift, but the ions do not because ions are not magnetized. Therefore resulting forces on the perturbation in LLR regime are in a similar charge separation of the MHD regime, but are much stronger. This occurs in higher instability growth rate than the conventional MHD-Rayleigh-Taylor instability. Huba *et al.* discussed about the LLR instability using Hall-MHD treatment [3]. According to their works, in LLR regime, i.e.,  $R_i/L_n \gg 1$ , in the limit of  $kL_n \gg 1$ , the linear Rayleigh-Taylor growth rate becomes

$$\gamma_{\text{LLR}} = kL_n \gamma_{\text{MHD}}, \quad (1)$$

where  $L_n = \partial \ln(n)/\partial x$  is a density gradient length,  $k$  is a wave number,  $\gamma_{\text{MHD}}$  is the usual MHD-Rayleigh-Taylor growth rate for  $kL_n \gg 1$ ,

$$\gamma_{\text{MHD}} = \sqrt{\frac{g}{L_n}}, \quad (2)$$

author's e-mail: nunami@rish.kyoto-u.ac.jp

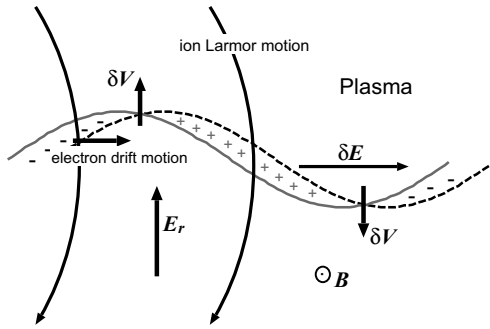


Fig. 1 Model of drift forces driving the growth of the LLR-regime Rayleigh-Taylor instability. Drift motion of the electron population is caused by large inward-directed electric fields generated by ion cyclotron motion with large Larmor radius.

and  $g$  is the plasma deceleration. This growth rate is much stronger compared with the conventional MHD-Rayleigh-Taylor growth rate.

### 3. Numerical simulation

#### 3.1 Simulation condition

To simulate the expansion of LPP in the LLR-regime with use of 3D PIC, we consider the spherical uniform dense neutral plasma,  $n_e = n_i$ , consisting of electrons and  $Z = 1$  ions with the plasma size parameter of  $\Lambda \simeq 62$ , where  $\Lambda \equiv R_0/\lambda_D$  is a plasma size parameter,  $R_0$  initial plasma radius,  $\lambda_D$  Debye length,  $\lambda_D = (\varepsilon_0 \kappa T_e / n_0 e^2)^{1/2}$ ,  $n_0$  and  $T_e$  are initial plasma density and electron temperature, respectively. The initial electrons have finite temperature  $T_e \neq 0$  with Maxwellian, and ion temperature is set to zero,  $T_i = 0$ . The external magnetic field is generated by a single coil and initial plasma cluster locates at the center of the coil. The ratio of the initial electron pressure to the magnetic pressure is chosen to be  $p_{e0}/p_B = n_0 \kappa T_e / (\mu_0 B_0^2 / 2) \simeq 14$  at the center of the coil. Definitions of initial density  $n_0$ , electron temperature  $T_e$  and magnetic field intensity  $B_0$  are given by the ratio. Number of electrons and ions is about from  $2 \times 10^5$  to  $1 \times 10^7$  each other, and the ion-electron mass ratio is set to  $m_i/m_e = 100$ .

At the present time, it is still very difficult to simulate with real plasma parameters if we use a present super computer. Therefore we use here relative and fictitious values of all simulation parameters, but with keeping relations of spatial and time scales to important physics to be the same. In the study of LPP expansion in a magnetic field, the relation of physical spatial and time scales of the problem are very important. In typical LPP-EUV experiments using Tin target, for example,  $R_0 = 5.0 \times 10^{-2}$  cm,  $B = 3$  T,  $n_0 = 10^{19}$  cm $^{-3}$  and  $T_e = 50$  eV. For the spacial relation in the experiment, Larmor radii of electrons and

Parameters	Simulation	Experiment
$m_i/m_e$	100	$2.16 \times 10^5$ (Tin ion)
$p_{e0}/p_B$	14	22.4
$\lambda_D$	$1.57 \times 10^{-2} R_0$	$1.67 \times 10^{-6}$ cm
$R_e$	$2.43 \times 10^{-1} R_0$	$7.95 \times 10^{-4}$ cm
$R_0$	$1.0 R_0$	$5.0 \times 10^{-2}$ cm
$R_B$	$2.4 R_0$	$1.4 \times 10^{-1}$ cm
$R_i$	$7.7 R_0$	$4.19 \times 10^0$ cm
$f_{pe}^{-1}$	$0.99 \times 10^{-2} \tau_s$	$3.52 \times 10^{-14}$ sec
$f_{ce}^{-1}$	$1.08 \times 10^{-1} \tau_s$	$1.19 \times 10^{-11}$ sec
$f_{pi}^{-1}$	$0.99 \times 10^{-1} \tau_s$	$1.64 \times 10^{-11}$ sec
$\tau_s$	$1.0 \tau_s$	$2.49 \times 10^{-8}$ sec
$f_{ci}^{-1}$	$1.08 \times 10^1 \tau_s$	$2.6 \times 10^{-7}$ sec

Table 1 Relative values of simulation parameters which we used in this paper. Relative relations for spatial and time scales are maintained compared with typical LPP-EUV experiment.

ions, magnetic confinement radius and initial plasma radius are hold the relation,  $\lambda_D < R_e < R_0 < R_B < R_i$ , where  $R_B$  is the magnetic confinement radius defined as  $R_B \equiv \sqrt[3]{3\mu_0 E_0 / 2\pi B_0^2}$  under the assumption of spherical symmetry,  $E_0$  is the total energy of the initial plasma and  $R_{e(i)}$  is electron (ion) Larmor radius. For the time scale relation, the plasma frequencies  $f_{pe(i)}$  and gyro frequencies  $f_{ce(i)}$  of electrons and ions, and ion expansion time defined as  $\tau_s \equiv R_0/c_{s0}$  are essential for the problem. The relation among them,  $f_{pe}^{-1} < f_{ce}^{-1} \sim f_{pi}^{-1} < \tau_s < f_{ci}^{-1}$ , is hold. The relations should be maintained in the simulations. In Table 1, we show relative values of simulation parameters which we used in this work.

#### 3.2 LLR instability

Figure 2 shows a snap shot of particle distributions for electrons and ions in a cross-field plane within a region of  $\pm R_0$  along the magnetic axis at  $f_{pi} t = 48.0$  obtained in our simulation results. In the figure, we can see that flute-like instability with mode number  $m = 8$  occurs in the electron surface, especially. With measured deceleration of the electrons,  $g = 1.29 \times 10^{-3} R_0 f_{pi}^2$ , wavelength and density gradient,  $kL_n = 1.33$  from the results, we can obtain theoretical LLR-instability growth rate from Eq.(1),  $\gamma_{LLR} = kL_n \gamma_{MHD} = 4.29 \times 10^{-2} f_{pi}$ , where the MHD-Rayleigh-Taylor instability growth rate in Eq.(2) is  $\gamma_{MHD} = (g/L_n)^{1/2} = 3.22 \times 10^{-2} f_{pi}$ . In Fig.3, we evaluated the time evolution of flute amplitude of the electron surface which are obtained by measuring distance between tips and bottoms of the flutes and averaging them. We obtained the instability growth rate from the result in linear phase,  $20.0 \lesssim f_{pi} t \lesssim 50.0$ ,  $\gamma_{sim} = 4.71 \times 10^{-2} f_{pi}$ . This agrees with the theoretical prediction of LLR-instability growth rate  $\gamma_{LLR}$ .

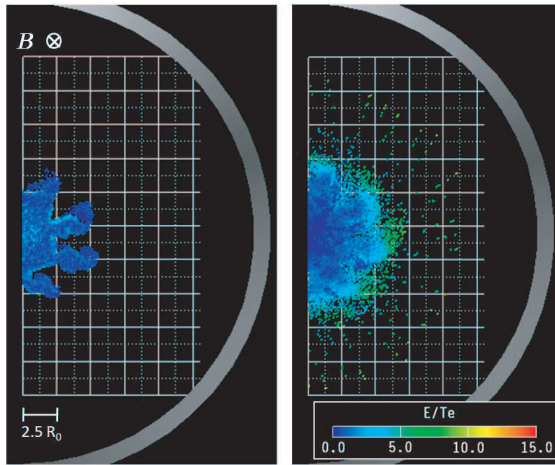


Fig. 2 A snap shot of particle distributions for electrons (left) and ions (right) in a half cross-field plane at  $f_{pi}t = 48.0$ . A ring represents the single magnetic coil.

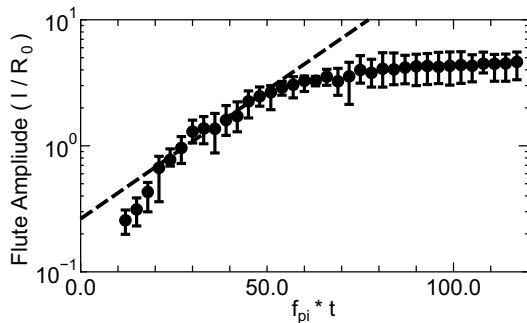


Fig. 3 Time evolution of flute amplitude of the electron surface. Dashed line shows the amplitude growth with  $\gamma_{sim} = 4.71 \times 10^{-2} f_{pi}$  for  $20.0 < f_{pi}t < 50.0$ .

Therefore we may conclude that the flute-like instability of the electron surface observed in our simulation results is the LLR-instability, certainly.

### 3.3 Flute curling

After the period of linear growth of the perturbation, the electron flutes begin to show some curvatures as in Fig.4(a) which is the electrons distribution at the same time of Fig.2. Ripin *et al.* discussed about the flute curling and proposed two mechanisms which could cause the curling [4] in Figs.4(b) and 4(c). The radial electric field mechanism, illustrated in Fig.4(b), may occur when the radial inward-directed electric field, which is the source of driving the LLR instability, is higher at tips of the flutes than in the bottom region of the flutes. The radial electric field would cause a shear in the electron  $\mathbf{E}_r \times \mathbf{B}$  drift velocity, hence, the flute curling occurs as in Fig.2(a). The other possible mechanism is the magnetic field gradient mechanism illustrated in Fig.4(c). In this mechanism, when the gradients of the magnetic field strength, which is gen-

erated by the expanding plasma excluding the magnetic field and creating diamagnetic cavity, are higher in the bottom region than in the tips region of the flutes, the magnetic field gradient causes a shear in the electron  $\nabla B$ -drift velocity, but the drift motion is caused with opposite direction with  $\mathbf{E}_r \times \mathbf{B}$  drift in the radial electric field mechanism. Fig.5 shows radial profiles of the radial electric field and the radial gradient of the magnetic field strength at  $f_{pi}t = 48.0$ . From the figure, we can see that differences of radial inward-directed electric field and the magnetic field gradients in bottom region and tips region of the flutes are generated indeed, i.e.,  $|\mathbf{E}_r|_{tip} > |\mathbf{E}_r|_{bot}$  and  $\nabla_r B^{tip} < \nabla_r B^{bot}$ . Therefore the observed curling phenomena of the electron flutes in Fig.4(a) are caused due to these two mechanisms by nonuniformity of the radial electric field and the radial gradient of the magnetic field strength.

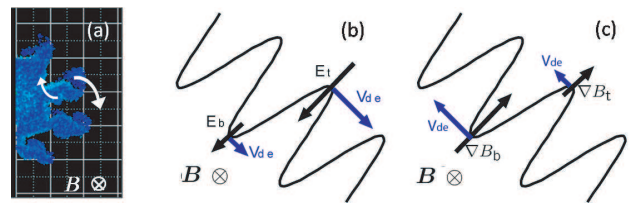


Fig. 4 Flutes curling of the electron surface (a) at the same time of Fig.2 and schematics of the flute curling mechanisms in the sense of electron drift motion, (b)  $\mathbf{E}_r \times \mathbf{B}$  drift and (c)  $\nabla B$ -drift. Shear of electron drift motion between flute tips and bottoms causes the flute curling.

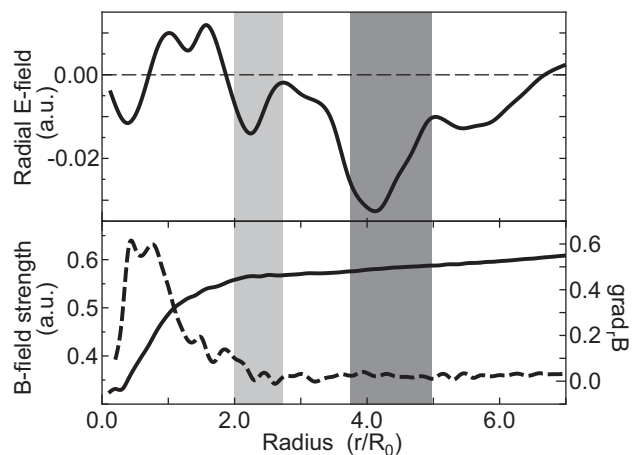


Fig. 5 Radial profiles of the radial electric field (top), the strength of the magnetic field (bottom; solid line) and the radial gradient of the magnetic field strength (bottom; dashed line) at  $f_{pi}t = 48.0$ . Hatched region with light gray indicates the region of the flute bottoms and with dark gray indicates the flute tips region.

### 3.4 Ion surface

In Fig.2, we can see that the instability seems to occur in inner radial region and not in outer region near the ion surface. To investigate the instability effect near the ion surface, we evaluated angular electric field, which is direct force to grow the perturbations, with distinction from inner to outer radial regions. Figure 6 shows the angular distributions of ions and angular electric field  $E_\theta$  at near the time of Fig.2 for the inner radial region ( $R < R_{\max}$ ) and the outer radial region ( $R > R_{\max}$ ) within a region of  $\pm R_0$  along the magnetic axis, where  $R_{\max}$  is the maximum ion Larmor radius which is obtained from observed energy spectrum of the ions,  $R_{\max} \simeq 7.5R_0$ . There exists a large angular disturbance of the ion density and corresponding angular electric field is generated in the inner region due to the LLR-Rayleigh-Taylor instability. However, no visible disturbances have been observed in the outer region for both ion density and the angular electric field. Therefore the instability occurs only in the inner region, but not in the outer region. Therefore ions can perform simple Larmor motion in the outer region.

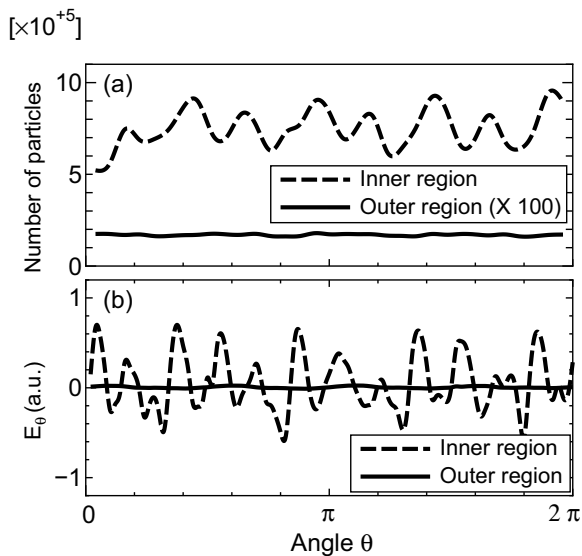


Fig. 6 (a) Ion angular distributions and (b) angular electric field  $E_\theta$  in inner radial region of  $R < R_{\max}$  (dashed line) and in outer region  $R > R_{\max}$  (solid line), where  $R_{\max}$  is the maximum ion gyro radius. Ion distributions in outer region with 100 times magnified scale.

### 4. Summary and discussion

We have investigated expansion dynamics of laser produced cluster plasma in an external strong magnetic field with ion large Larmor radius by 3D full PIC simulation. In LLR regime, the growth mechanism of the instability is quite different from conventional MHD-Rayleigh-Taylor instability. The LLR instability is caused by inward-directed radial electric field

generated by unmagnetized ions Larmor motion. We evaluated the growth rate of the LLR instability during the linear phase and confirmed that it agrees with theoretical prediction of the LLR-instability which is higher than the growth rate of conventional MHD-Rayleigh-Taylor instability. And we observed the curling phenomena of the electron flute which is caused by the shear of the electron drift velocity by  $\mathbf{E}_r \times \mathbf{B}$  and  $\nabla B$ -drift between in the tips and bottoms of the flutes. The shear is generated by nonuniform radial electric field and the gradient of the magnetic field strength. Instability effects at ion surface were also evaluated. Because the electrons are magnetized while the ions are not magnetized, the instability occurs in only inner radial region near the electron surface, does not occur in outer radial region near the ion surface.

In the development of LPP-EUV light source which is one of the most promising technology for next generation high volume patterning lithography [1, 5], the mitigation of the energetic ions is one of the critical issues that should be overcome. Magnetic field mitigation is a candidate concept for the mitigation of the ion debris [6]. LPP expansion phenomena in this scheme are just in LLR regime. Therefore the fact that LLR instability does not occur at the ion surface is good to develop the LPP-EUV light source using the mitigation scheme without a care for the instability [7]. The nonlinear stage of the LLR instability may have some very unusual behaviors and the phenomena should be explored with further analysis.

### Acknowledgment

A part of this work was performed under the auspices of Leading Project promoted by MEXT and Japan Science and Technology Agency, CREST.

- [1] W.T. Silfvast and N.M.Ceglio, Appl. Opt. **32**, 6895 (1993).
- [2] L. Rayleigh, Proc. London Math. Soc. **14**, 170 (1883); G.I. Taylor, Proc. R. Soc. London Ser. A **223**, 348 (1950).
- [3] J.D. Huba, A.B. Hassam and P. Satyanarayana, Phys. Fluids B **1**, 931 (1989); A.B. Hassam and J.D. Huba, Geophys. Res. Lett. **14**, 60 (1987).
- [4] B.H. Ripin, J.D. Huba, E.A. McLean, C.K. Manka, T. Peyser, H.R. Burris and J. Grun, Phys. Fluids B **5**, 3491 (1993).
- [5] F. Jin and M. Richardson, Appl. Opt. **34**, 5750 (1995); R.C. Spitzer, *et al.*, J. Appl. Phys. **79**, 2251 (1996); A. Shimoura, *et al.*, Appl. Phys. Lett. **75**, 2026 (1999); I.W. Choi, *et al.*, J. Opt. Soc. Am. B **17**, 1616 (2000); Y. Shimada, *et al.*, Appl. Phys. Lett. **86**, 051501 (2005); T. Aota and T. Tomie, Phys. Rev. Lett. **94**, 015004 (2005); P. Hayden, *et al.*, Proc. SPIE **5751**, 919 (2005).
- [6] S.S. harilal, *et al.*, J. Appl. Phys. **98**, 036102 (2005); S.S. harilal, *et al.*, Appl. Phys. B **86**, 547 (2007).
- [7] M. Nunami, A. Takata and K. Nishihara, Jour. Phys. Conf. Ser. **112**, 042061 (2008).